Measured and calculated SF_6^- collision and swarm ion transport data in SF_6-Ar and SF_6-Xe mixtures

M. Benhenni,[1] J. de Urquijo,[2] M. Yousfi,[1,*] J. L. Hernandez-Ávila,[3] N. Merbahi,[1] G. Hinojosa,[2] and O. Eichwald[1]
[1]*Université Paul Sabatier, CPAT, UMR 5002 du CNRS, 118 route de Narbonne, 31062 Toulouse cedex, France*
[2]*Centro de Ciencias Físicas, Universidad Nacional Autónoma de México, Apartado Postal 48-3, 62251, Cuernavaca, Mor., Mexico*
[3]*Universidad Autónoma Metropolitana, CBI-Energía, Av. San Pablo 180, 02200 México, D. F., Mexico*
(Received 12 October 2004; published 17 March 2005)

The measurement of the mobility of SF_6^- in the mixtures SF_6-Ar and SF_6-Xe is reported over the density-reduced electric field strength E/N 1–180 Td (1 Townsend$=10^{-17}$ V cm^2), from a time-resolved pulsed Townsend technique. Simultaneously, the mobility of SF_6^- in the same binary mixtures has been calculated from a set of collision cross sections for SF_6^--Ar, SF_6^--Xe, and SF_6^--SF_6 using a Monte Carlo simulation procedure for ion transport. The good agreement between measured and calculated mobilities in these gas mixtures has led us to conclude that the validation of our cross section sets is confirmed. The elastic collision cross section, a predominant process for ion energies lower than about 10 eV, was determined from a semiclassical JWKB approximation using a rigid core potential model for the ion-neutral systems under consideration. This elastic cross section was then added to several other inelastic collision cross sections found in the literature for ion conversion, electron detachment of SF_6^- and charge transfer. Moreover, the calculations of the mobility and the ratios of the transverse and longitudinal diffusion coefficients to the mobility were extended into a much wider E/N range from 1 to 4000 Td. Additionally, we have also calculated the energy distribution functions and the reaction coefficients for ion conversion and electron detachment. Finally, we have shown that the range of validity for the calculation of the mobility in gas mixtures from Blanc's law is only valid for the low E/N region, where the interaction is dominated by elastic collisions and the ion distribution function remains essentially Maxwellian.

DOI: 10.1103/PhysRevE.71.036405 PACS number(s): 52.20.Hv, 51.50.+v, 52.25.Fi

I. INTRODUCTION

Gas mixtures involving sulfur hexafluoride (SF_6) are commonly used in numerous applications such as high voltage engineering, plasma processing rare gas-halide excimer lasers, and many more (see, e.g., [1–4]). Also, these mixtures have been suggested as possible substitutes to using pure SF_6, because of its very high global warming potential of the latter, which amounts to be nearly 24 000 times that of CO_2, the most abundant greenhouse gas in the atmosphere [3]. Many of these applications involve an electrical discharge environment under nonthermal plasma conditions, mainly governed by the electron and ion transport in a strong, nonuniform, space charge dominated electric field. Thus, in order to optimize these plasma processes, a better understanding of the basic phenomena and more comprehensive knowledge of the electron or ion-molecule swarm and cross section data are strongly needed. These fundamental sets of data are regarded to be rather well known for the case of electrons in SF_6 and some of its mixtures [2,5–8], whereas the basic data for SF_6 ion-molecule interactions are comparatively scarce, and more particularly for the gaseous mixtures involving SF_6 [8].

The only available measured ion swarm data deal mostly with the interaction of SF_6 ions with only a few pure gases and some specific gas mixtures (see, e.g., [8,9]). On the other hand, for the case of ion interactions with SF_6, the only available cross sections in the literature for SF_6^- (the major negative ion produced in a nonthermal discharge in SF_6) are those concerning the inelastic processes of electron detachment, ion conversion and charge transfer [10]. There are no cross section data on the elastic processes which, as is known, largely govern the ion transport in nonthermal plasmas.

As regards the calculations, the aim of this work is to first determine the elastic cross sections of SF_6^- in collision with pure SF_6, Ar, and Xe in the gas phase, followed by the calculation of the mobility and the longitudinal and transverse components of the diffusion tensor of SF_6^- in the SF_6-Ar and SF_6-Xe mixtures. The resulting sets of elastic and inelastic collision cross sections for these pure gases become validated from the systematic comparison between the ion mobility calculated from an optimized Monte Carlo method [11] and the time-resolved measurements of SF_6^- in Ar and Xe and in their binary mixtures with SF_6. Moreover, the ion mobility in a gas mixture is usually calculated from restrictive linear approximations. Thus, the present paper also aims at discussing the validity of such linear approximation in these gas mixtures, and to extend the range of the density-reduced electric field strength E/N, well above that hitherto measured, where no mobility data are available in the literature at all. These mobility and diffusion coefficients are necessary in electrical fluid models for the modeling of numerous nonthermal plasma discharges over wide ranges of E/N.

Following this introduction, Sec. II is devoted to an overview of the experimental time-resolved technique used to

*Author to whom correspondence should be addressed at Université Paul Sabatier, CPAT, UMR 5002 du CNRS, 118 route de Narbonne, 31062 Toulouse Cedex 4, France. FAX: 05 61 55 63 32. Email address: yousfi@cpat.ups-tlse.fr

measure the mobility of SF_6^- in the binary mixtures SF_6-Ar and SF_6-Xe. Section III describes the calculation of the elastic collision cross sections, based on the JWKB approximation, by using a specific interaction potential model that is well adapted to ion-neutral polyatomic interaction systems for both the symmetric and asymmetric cases. The elastic cross sections are calculated for the collision of SF_6^- with pure SF_6, Ar, and Xe. The validation of the cross section sets is discussed in Sec. IV for the case of the mobility of SF_6^- in SF_6, Ar, and Xe. The validation analysis is then continued for the mobility of SF_6^- in the binary mixtures SF_6-Ar and SF_6-Xe over the same E/N range and SF_6 mixture compositions used in the measurements with the gas mixtures. Then for a wide E/N range (i.e., up to a few thousands of Td) the mobility and diffusion (transverse and longitudinal) data of SF_6^- ion are given for the case of the different gas mixtures, including the calculations of ion conversion and detachment coefficients. Finally, the E/N ranges over which the elastic collisions predominate over the inelastic ones are discussed in terms of the calculated energy distribution functions. Additionally, the validity of using Blanc's law to evaluate the mobility of SF_6^- in these mixtures is discussed both at low and high E/N regimes.

II. EXPERIMENTAL DETAILS

The time-resolved pulsed Townsend method relies on the measurement of the total displacement current due to electrons and ions drifting through a parallel-plate capacitor [12,13]. The discharge is initiated by the instantaneous release of photoelectrons from the cathode by the action of a very short flash of UV light. These photoelectrons move towards the anode by the action of the uniform electric field between the electrodes. For the present experiment, in which ionization processes are either absent or negligible in comparison with electron attachment, the electrons will attach readily to the molecules, giving rise to a measurable current in the external circuit given by [12,14]

$$i_e(t) = \frac{n_0 q_0}{T_e} \exp(-\eta v_e t), \tag{1}$$

where n_o is the photoelectron number, q_o is the ion charge, η is the electron attachment coefficient, v_e is the electron drift velocity, and $T_e = d/v_e$ (d being the gap spacing) is the electron transit time. Accordingly, the negative ion current during the electron transit is [12,14]

$$i_n(t) = \frac{n_o q_o}{T_n}[1 - \exp(-\eta v_e t)], \tag{2}$$

where $T_n = d/v_n$ is the negative ion transit time and v_n is the negative ion drift velocity. Under the special conditions of strong attachment, occurring at low E/N, and for the high pressures used in these experiments (50 up to 200 torr), the negative ion current will reach its maximum value well before the electron transit time T_e. During the ionic drift regime $T_e < t < T_n$, the negative ion current is [12,14]

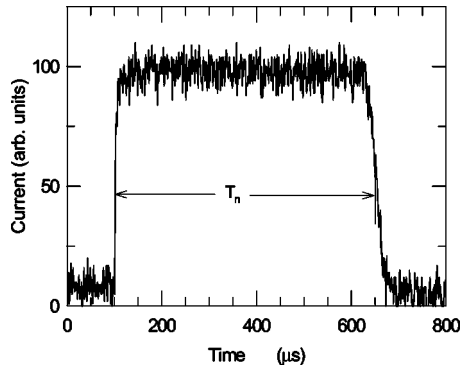

FIG. 1. Negative ion transient in SF_6-Xe for 10% SF_6. The conditions of the transient are $E/N = 30$ Td, $d = 3.1$ cm, and $N = 3.24 \times 10^{18}$ cm^{-3}. The transit time T_n is indicated. The resulting drift velocity is 5.61×10^3 cm s^{-1}, and the reduced mobility is $K_0 = 0.695$ cm^2 V^{-1} s^{-1}.

$$i_n(t) = \frac{n_o q_o}{T_n}\{1 - \exp[-\eta(d - v_n t)]\}. \tag{3}$$

Moreover, for large η and $d - v_n t > 0$, the exponential term in Eq. (3) is very small as compared to unity, so that this equation can be approximated to

$$i_n(t) \approx \frac{n_o q_o}{T_n} \tag{4}$$

for $T_e < t < T_n$, which means that the displacement current remains essentially constant during the ion drift regime. On physical grounds, the above equation describes the motion of a negative ion lamina that was formed very close to the cathode due to strong attachment, and travels toward the anode without losing its identity, since ion diffusion has been neglected. Figure 1 shows a sample transient from which the ion transit time can be readily measured. Finally, the drift velocity is evaluated by

$$v_n = d/T_n. \tag{5}$$

and from it the reduced mobility

$$K_o = \frac{v_n}{N_o} \frac{N}{E}, \tag{6}$$

where $N_0 = 2.69 \times 10^{19}$ cm^{-3} is the gas density at STP.

The apparatus used for this study has been described in detail elsewhere [13,15]. The UV light pulse was produced by a nitrogen laser (337 nm, 1 ns width, 1.4 mJ, maximum output energy) that released the photoelectrons from an aluminum cathode. The anode holds a central hole of 1 cm in diameter, covered by a flat OHFC copper mesh of 75 lines/mm, to allow the passage of the UV light. The gap distance was kept fixed at $d = 3 \pm 0.001$ cm. The base vacuum pressure was typically 7×10^{-7} torr. The gas pressure was measured by a 0–1000 torr with 0.02% accuracy, and its temperature with 0.1 C resolution. The measurements were performed at room temperature over the range 296 up to 303 K. The maximum error in the setting of E/N is then estimated to be less than 0.3%. The ionic avalanche was detected by a transimpedance amplifier with a gain of 10^7 V/A

and 400 kHz bandwidth. The SF_6-rare gas mixture was prepared inside the discharge vessel by first injecting the minority gas; normally, the initial gas pressure was in the range 50–200 torr. The stated purities of SF_6, Ar, and Xe were 99.8%, 99.99%, and 99.9999%, respectively. The overall precision of the measured mobility is 2–4 %.

The use of aluminum as the cathode material has the advantage that its work function is very close to that of the energy of the laser photons (3.69 eV). Thus, the electrons would be released from the cathode with virtually zero translational energy, so that the electron capture process would occur very efficiently with a very high cross section of the order of 10^{-14} cm^2. Even though the present apparatus lacks mass analysis, we have previously given a number of reasons to support the fact that it is perfectly possible to carry out negative-ion transport studies reliably, provided that the ranges of operation are such that there exists the certainty that only one majority species forms very close to the anode and drifts across the gap [15]. In this respect, the negative ions can be formed in SF_6 by resonant (SF_6^-) and dissociative electron attachment (SF_5^-,F^-, and other minority species), and by ion-molecule reactions [2]. Since the SF_6 molecule has a very large electron attachment cross section σ_a for slow electrons (for instance, $\sigma_{at,SF6-} \sim 8\times10^{-13}$ cm^2 for 100 μeV and $\sigma_{at,SF6-} \sim 10^{-16}$ cm^2 for 240 meV; see, e.g., [2]), the majority ion is SF_6^-, followed by SF_5^-, which is formed by dissociative attachment, its cross section peaking at ~0.3 eV with $\sigma_{dat,SF5-} \sim 4\times10^{-16}$ cm^2. Thus, even for electron impact energies of $\varepsilon = 100$ meV, SF_6^- is being produced predominantly, since $\sigma_{at,SF6-}/\sigma_{dat,SF5-} \sim 30$. Therefore, for the mixtures under study, and for the relatively small values of E/N (i.e., low mean electron energies), the negative ion avalanche signal can be ascribed to the presence of SF_6^-, at least as the overwhelming majority species over such electron energy range. On the other hand, over the relatively high pressure range used in this experiment, even for relatively small SF_6 concentrations in the mixture of say, 10% (5–20 torr SF_6), with an attachment rate constant of $k_{att} \sim 1.41\times10^{-7}$ cm^3 s^{-1} for $\varepsilon = 0.1$ eV, $N = 3.3\times10^{17}$ cm^{-3}($p = 10$ torr), this gives an attachment frequency of $k_{att}N = \eta v_e \sim 4.6\times10^{10}$ s^{-1}. Inserting this value into Eq. (1), we see that 99.4% of the initial photoelectron population produced at the cathode surface has been attached to the SF_6 neutrals to form SF_6^- in only 100 ps. Considering a typical electron drift velocity of the order of 5×10^6 cm s^{-1}, and a gap spacing of 3 cm, the electron transit time is $T_e = 600$ ns, thereby indicating that electron attachment in this experiment proceeds very readily during the very first stages of electron motion, leading to the formation of a lamina of negative ions very close to the cathode, as is seen from Eq. (2). Furthermore, even for average electron energies well above thermal, most of the photoelectrons are captured just after their release, well before they relax and acquire their drift velocity, according to the applied E/N value. This in turn means that, for the relatively high pressures used in this study, a photoelectron could be captured by a SF_6 molecule during the first collisions, well before it attains its drift velocity. The only exception to the above is the case for the mobility of SF_6^- in pure Ar or Xe. In our case, we used only a few ppm SF_6 diluted in Ar or Xe. Thus we could only measure this drift velocity over a very reduced range of E/N since the SF_6^- acquires a fairly high drift velocity that would eventually lead it to breakup into SF_5^-+F, as can be seen from Figs. 3(a)–3(c), for the cross sections leading to the above products of SF_6^- with SF_6, Ar, and Xe, respectively. Notice that, in general, above 10 eV, the dissociation cross sections are as high as 10^{-15} cm^2. Notice also that the quite hot (i.e., with about 1 eV) electrons susceptible to be released from the SF_6^- ion by detachment would be most likely recaptured after a few mean free paths, or, when the SF_6 share in the mixture is low, to gain enough energy from the field to create for either SF_5^- or F^- from electron impacts with SF_6. However, the latter case may be neglected over the present work E/N range, because of the very low SF_6^- detachment cross sections in the corresponding ion energy range [see Figs. 3(a)–3(c)]. Further evidence of the above will be apparent below, from the very good agreement between measured and calculated mobilities for SF_6^- drifting in the SF_6-Ar and SF_6-Xe mixtures. Previous values of the mobility of SF_6^- in SF_6^--Ar presented in a conference [16] are superseded by the present ones and therefore the former data should be disregarded.

III. COLLISION CROSS SECTIONS AND METHOD OF CALCULATION

The calculation of the mobility of SF_6^- in the present binary SF_6-rare gas mixtures with the optimized Monte Carlo simulation procedure [11] demands the knowledge of a very complete set of elastic and inelastic cross sections. In what follows some details concerning the determination and origin of both elastic and inelastic collision cross sections are given.

It is known that under nonthermal plasma discharge conditions, and for ion energies not exceeding a few tenths of eV, the main collision process that governs ion drift and diffusion of SF_6^- in the rare gases at large is the elastic one. The collision cross section Q_m associated with the elastic process for SF_6^- is unknown and therefore needs to be estimated from calculations requiring the knowledge of the interaction potential. Several interaction potentials have already been used to describe the ion-atom interactions, in contrast with the polyatomic ion-molecule(atom) systems which are less studied. However, there are previous studies concerning the polyatomic ion-molecule system for the case of flue gases, such as for example, CO_2^+ or H_2O^+ in collision with several other molecules [17,18]. The interaction potential developed by Mason *et al.* [19] was used in previous calculations [17,18], and has been adapted in the present work. This rigid core potential corresponds to the algebraic sum of one repulsive and one attractive term. The adaptation of this potential $V(r)$ for the SF_6^- ion in the rare gases consists of choosing the most adequate exponent for the repulsive term, as well as the other three parameters (i.e., r_m, ε_w, and a). Thus $V(r)$ is written as

$$V(r) = \varepsilon_w \left\{ 2\left(\frac{r_m - a}{r - a}\right)^6 - 3\left(\frac{r_m - a}{r - a}\right)^4 \right\}, \tag{7}$$

where ε_w is the potential well depth, r_m the position of the potential minimum, and r the internuclear distance. The rigid

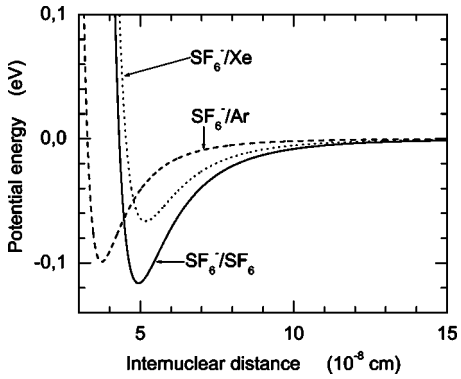

FIG. 2. The interaction potentials for SF_6^--SF_6, SF_6^--Ar, and SF_6^--Xe, calculated from Eq. (7).

core diameter a is the shift induced by the ion on the neutral between its center of mass and its center of charge. The parameter a is determined by equating the attractive term of the interaction potential with the classical attractive polarization term, thereby leading to [17,19]

$$3\varepsilon_w(r_m - a)^4 = C_A^2 \alpha_B, \tag{8}$$

where α_B is the polarizability of the neutral (rare gas atom or SF_6 molecule), and C_A the ionic charge state (C_A=−1 for SF_6^-). Figure 2 shows a plot of the three calculated interaction potentials of SF_6^- with SF_6, Ar, and Xe. The particular values obtained for the potential parameters of the three different interaction systems are summarized in Table I. One can note in Fig. 2 the three typical regions of the interaction potential. Namely, the short internuclear distance range corresponding to the high energy region where the interaction potential is dominated by the repulsion between the nuclei. This is followed by an intermediate energy region where the electrostatic forces of both the nuclear repulsion on the one hand and on the other hand the attraction forces between the ion and the dipole moment induced on the neutral are influential. And finally in the lower energy region corresponding to the long internuclear distance range, the latter attraction forces are predominant.

Once the potential $V(r)$ is known from the previous relations, the elastic collision cross section Q_m, which is the dominant collision process in the case of SF_6^-, can be calculated first from a simplified classical technique [20]. This latter method has the unavoidable drawback brought about by a singularity problem that cannot be eliminated, giving rise to a resonance phenomena that produces an oscillation on the differential cross section. It is also possible to calculate Q_m from a complex quantum method, capable of rendering accurate collision cross sections, with the disadvantage of demanding a very long computing time [21]. An alternate method, of good accuracy over the present energy range, from thermal up to a few tens of eV, that provides the values of Q_m within a reasonable computing time, is the semiclassical formalism used in the present work. This is based on the JWKB approximation for the calculation of the phase shift δ_l induced by the rigid core interaction potential $V(r)$ on the diffused wave with respect to the incident wave [17,22,23]

$$\delta_l \approx \delta(b) = k\int_{r_0}^{\infty} dr\left(1 - \frac{b^2}{r^2} - \frac{V(r)}{\varepsilon_r}\right)^{1/2} - k\int_{b}^{\infty} dr\left(1 - \frac{b^2}{r^2}\right)^{1/2}, \tag{9}$$

with the impact parameter

$$b = \frac{1 + 1/2}{k}. \tag{10}$$

The wave number k of the relative motion is proportional to the relative ion energy ε_r, and l is the angular momentum quantum number. Then, from the phase shift δ_l, the elastic collision cross section for momentum transfer can be calculated as

$$Q_m(\varepsilon_r) = \frac{4\pi}{k^2}\sum_{l=0}^{\infty}(l+1)\sin^2(\delta_{l+1} - \delta_l). \tag{11}$$

For the determination of the ion swarm transport coefficients from a Monte Carlo simulation, in addition to Q_m, one also needs the relevant inelastic collision cross sections. In our case, ion conversion, charge transfer, and electron detachment may also take place, mostly for ion energies exceeding 1 eV; these cross sections were taken in principle from scarce data available in the literature [10]. Thus we have, for the SF_6^--X system, where X stands for SF_6, Ar, or Xe,

$$SF_6^- + X \rightarrow SF_5^- + F + X, \tag{12}$$

$$SF_6^- + X \rightarrow SF_5 + F^- + X, \tag{13}$$

$$SF_6^- + X \rightarrow e + SF_6 + X, \tag{14}$$

for ion conversion to SF_5^-, F^-, and electron detachment, respectively. Additionally, the reaction

$$SF_6^- + SF_6 \rightarrow SF_x^- + F_{(6-x)} + SF_6 \tag{15}$$

is the dissociative charge transfer for $x<5$.

These inelastic collision cross sections for the above processes, along with the elastic ones are plotted in Figs. 3(a)–3(c) for SF_6^--SF_6, SF_6^--Ar, and SF_6^--Xe systems, respectively. Since the inelastic cross sections for ion conversion to F^-, ion conversion to SF_5^-, charge transfer and electron detachment have not been measured for SF_6^- energies below 1 eV, these were extrapolated down to their respective thermodynamic thresholds of 2, 1.35, and 3 eV [10]. For the case of electron detachment, the respective cross section

TABLE I. The position of potential minimum r_m, the depth of the potential well ε_w, and the rigid core diameter a of the interaction potentials $V(r)$ for the systems SF_6^--SF_6, SF_6^--Ar, and SF_6^--Xe.

Collision system	r_m(Å)	ε_w(eV)	a(Å)
SF_6^--SF_6	4.94	0.12	0.88
SF_6^--Ar	3.74	0.10	0.05
SF_6^--Xe	5.17	0.07	0.03

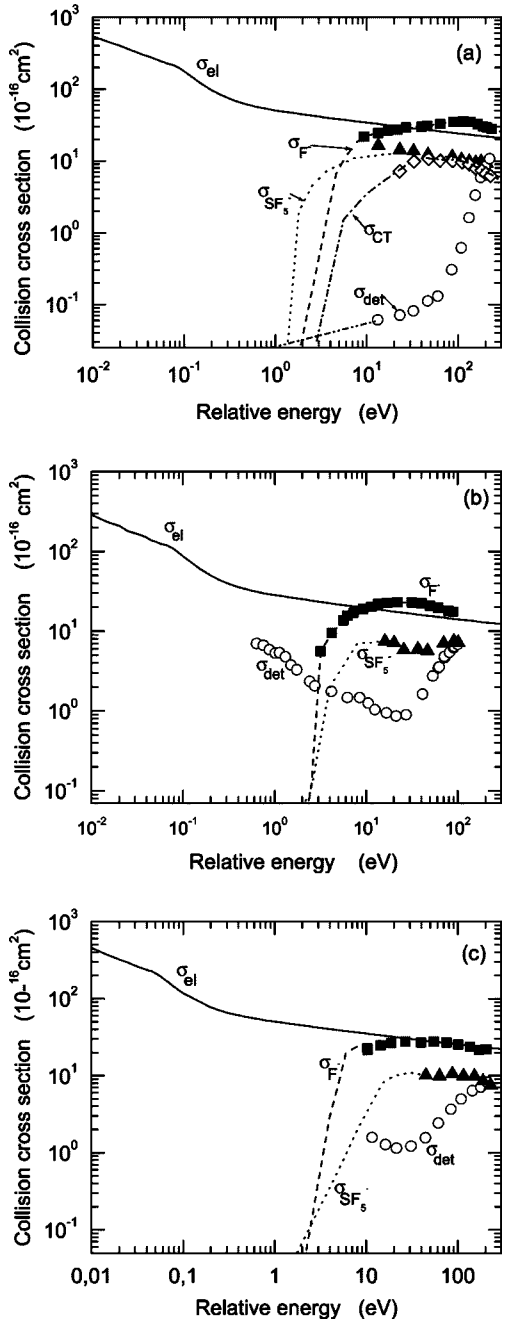

FIG. 3. (a) Set of cross sections for SF_6^--SF_6 system. Full line: calculated elastic cross section σ_{el}; the symbols represent the measured data taken from Ref. [8]; $\sigma(F^-)$: ion conversion to F^-; $\sigma(SF_5^-)$: ion conversion to SF_5^-; σ_{CT}: charge transfer; σ_{det}: electron detachment form SF_6^-. The broken lines represent the extrapolations of the inelastic cross sections at lower energies. (b) Set of cross sections for SF_6^--Ar system. Full line: calculated elastic cross section σ_{el}; the symbols represent the data taken from Ref. [8]; $\sigma(F^-)$: ion conversion to F^-; $\sigma(SF_5^-)$: ion conversion to SF_5^-; σ_{det}: electron detachment form SF_6^-. The broken lines represent the extrapolations of the inelastic cross sections at lower energies. (c) Set of cross sections for SF_6^--Xe system. Full line: calculated elastic cross section σ_{el}; the symbols represent the data taken from Ref. [8]; $\sigma(F^-)$: ion conversion to F^-;$\sigma(SF_5^-)$: ion conversion to SF_5^-; σ_{det}: electron detachment form SF_6^-. The broken lines represent the extrapolations of the inelastic cross sections at lower energies.

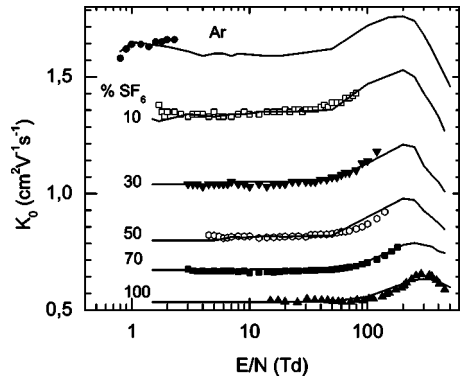

FIG. 4. Reduced mobility data of SF_6^- in SF_6-Ar mixtures for different fractions of SF_6; symbols: measurements; solid lines: calculations. The experimental values for pure SF_6 were taken from the drift tube-mass spectrometer measurement of Ref. [30].

does not vanish even at energies smaller than the electron affinity of SF_6^- (1.1 eV) [10], which is indicative of the contribution to the cross section from the $(SF_6^-)^*$ excited ion states. Thus, we extrapolated the electron detachment cross section to energies even lower than those given by Wang *et al.*, so that our calculated reaction coefficients coincide with the measured ones at $E/N=433$ Td [10]. In all three cases, we observe that the calculated elastic cross section for momentum transfer dominates for SF_6^- energies lower than 1 eV.

Finally, the present procedure of cross section determination can be summarized as follows. For a given system (e.g., SF_6^--Ar), we start from an initial pair of the potential parameters (r_m and ε_m) which give us the rigid core diameter a [Eq. (8)]. Then, the corresponding momentum transfer cross section is calculated using the JWKB approximation [Eqs. (9) and (11)]. The cross section set is then completed by adding the inelastic cross sections (described by reactions 12 up 15) before performing the Monte Carlo simulations that allow the first comparison between the measured and calculated ion swarm parameters. In the case of a disagreement higher than the experimental uncertainty (e.g., 3% for ion mobility), the potential parameters are fitted up to obtain a good coherence between measurements and calculations. The cross section sets thus obtained for each individual system are directly used without any new fitting for the gas mixtures.

IV. RESULTS

A. Validation and discussion

Figures 4 and 5 show the calculated mobilities of SF_6^- in the binary mixtures SF_6-Ar and SF_6-Xe for different fractions of SF_6 in these gas mixtures, along with the measured ones. The measured mobilities for SF_6^- in pure SF_6 shown in Figs. 4 and 5 were taken from a drift tube-mass spectrometer measurement of proven reliability [30], and a very good agreement is seen between measurement and calculations. In our experiment, the lower E/N end was dictated mostly by the detectability of the signal. As is noted in Fig. 1, the drift velocity is inversely proportional to the transit time of the

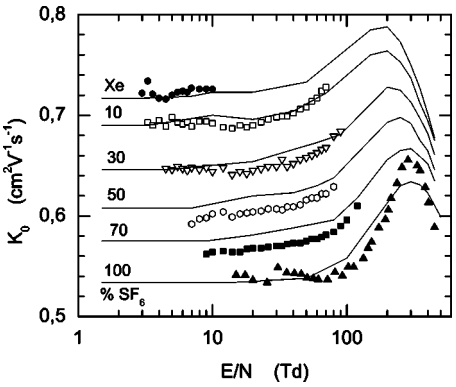

FIG. 5. Reduced mobility data of SF_6^- in SF_6-Xe mixtures for different fractions of SF_6; symbols: measurements; solid lines: calculations. The experimental values for pure SF_6 were taken from the drift tube–mass spectrometer measurement of Ref. [30].

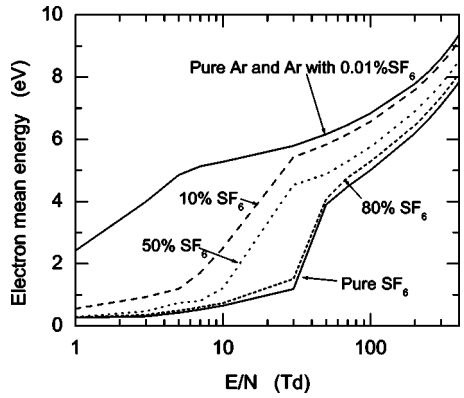

FIG. 6. The mean energy of electrons as a function of E/N for different fractions of SF_6 in the SF_6-Ar gas mixture.

ion across the gap. Thus, as the share of SF_6 in the mixture increases, the mobility of the ion becomes smaller and, for fixed E/N, the ion transit time becomes larger, thereby limiting our measurement. This is nicely shown in both Figs. 4 and 5 by the fanning out of the mobility curves to higher E/N ending values as the SF_6 content in the mixture increases. On the other hand, the higher E/N limit was restricted to mostly the fairly constant portions of the mobility curves and their rising portions in which both measurement and calculations agreed well. It has already been discussed that at relatively high values of E/N both electron impact dissociation and ion conversion leading to SF_5^- become important.

The Monte Carlo calculations were performed over a range of E/N from 3 Td to 400 Td, which is slightly wider than that covered by the measurements. The mobility curves bear the typical shape, consisting of a plateau at low E/N, due to the influence of the attractive part of the interaction potential arising from the polarization exerted by the ion upon the neutral. In the intermediate energy range, we identify a maximum, and then a rapid decrease of the mobility at high E/N due to the dominant, repulsive part of the interaction potential arising from short-range forces. These three different regions on the mobility curve can be related to the corresponding three different portions of the elastic cross section limited by a change in the slope, as displayed in Figs. 3(a)–3(c).

The good agreement observed in Figs. 4 and 5 between the measured and calculated mobilities of SF_6^- in the SF_6–rare-gas mixtures, where the relative deviation between them does not exceed 3%, well within experimental uncertainties, leads us to regard the present cross section sets used in the calculation as validated. For the SF_6^--Ar case, it is important to note that the measured mobility data are constrained to a very narrow E/N range (0.8–2.3 Td) in order to avoid any substantial production of SF_5^- from dissociative electron attachment, thereby keeping SF_6^- as the predominant ion drifting across the gap. Indeed, since the SF_6 negative ions are produced by electron attachment, when the SF_6 concentration in the mixture with Ar is, say, less than 1%, even at small values of E/N the electrons acquire a fairly high energy around 2.5 eV for $E/N=1$ Td, as is shown in Fig. 6. In contrast, for either pure SF_6 or SF_6-Ar mixtures in which the share of SF_6 exceeds 10% of the whole, the mean electron energy becomes sufficiently low ($\approx$0.5 eV) so as to preclude substantial formation of SF_5^-. The reason for this, as is well known, is that SF_6^- formation by electron impact has a very high attachment cross section $\sigma_{at,SF6^-}$ at very low electron energies near zero eV, and it becomes negligible above about 0.7 eV, while the dissociative electron attachment cross section $\sigma_{dat,SF5-}$ becomes higher than $\sigma_{at,SF6^-}$ only above around 0.2 eV, to be relayed by F^- formation by electron attachment above roughly 2 or 3 eV (see, e.g., [2]). As it was explained in the experimental section, the mobility of SF_6^- in the pure gas was measured by adding only small amounts, in the ppm range, of SF_6 into the rare gas. In Fig. 6 we show that the mean electron energy for 0.01% SF_6 in Ar remains essentially equal to that of pure Ar, which means that it is only safe to measure the mobility of the assumed SF_6^- at very low values of E/N. Notice that this restriction is almost eliminated for the other SF_6-Ar mixtures for which the share of SF_6 exceeds or equals 10%, showing an excellent agreement between measured and calculated mobilities. The previous simple observations based on the magnitude of the attachment cross section ($\sigma_{at,SF6-}$ or $\sigma_{at,SF5-}$) as a function the incident electron energy applied to Ar with a small admixture of SF_6 (i.e., 0.01%) concerning the dominant ion (either SF_6^- or SF_5^-) are no longer valid in pure SF_6 since the negative ions formed at different E/N or energy (for example lower or higher for 2 eV corresponding roughly to 30 Td) are subject to complex and significant ion conversion processes as described for instance, by McGeehan *et al.* [24]. Indeed, these authors showed that in pure SF_6, the SF_6^- ion has a dominant concentration in comparison to SF_5^- and F^- up to about 300 Td. However, such ion conversions are certainly much lower in the case of Ar with only a small admixture of SF_6. In this latter case, only the SF_6^- detachment cannot be negligible, although only for higher E/N values. Furthermore, it is interesting to observe that the results shown in Fig. 6 are coherent with those of Hunter *et al.* [7].

Concerning the ion collision cross section validation at thermal energies, the extrapolated, zero-field mobilities of SF_6^- in the pure gases SF_6, Ar, and Xe were estimated to be

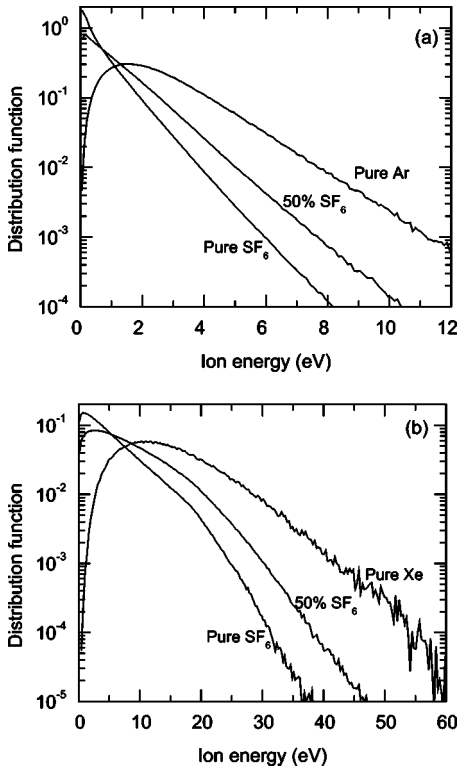

FIG. 7. (a) The energy distribution function of SF_6^- in SF_6, Ar, and the SF_6-Ar (50:50) mixture for $E/N=400$ Td. (b) The energy distribution function of SF_6^- in SF_6, Ar, and the SF_6-Xe (50:50) mixture for $E/N=2000$ Td.

0.53, 1.61, and 0.71 $cm^2\ V^{-1}\ s^{-1}$, respectively, and are in excellent agreement with the experimental ones.

It is important to note that the present calculations show no significant contribution of the inelastic cross sections on the SF_6^- mobility over a quite wide E/N range up to 400 Td. This is illustrated more particularly in Fig. 7(a), where the energy distribution function of SF_6^- in pure SF_6, SF_6-Ar (50:50) and pure Ar are plotted as a function of ion energy for $E/N=400$ Td, which is the upper limit range chosen for comparing the ion mobilities of SF_6^- in SF_6-Ar and SF_6-Xe, shown in Figs. 4 and 5, respectively. It is clearly seen in Fig. 7(a) that the mean energy of the bulk of ions, which are influential in either the measurement or on the calculation of the transport coefficients, does not exceed a few eV. Thus it seems that this rather low, limited energy region of the distribution function contributes very little to the appearance of the inelastic processes such as ion conversion, charge transfer, and electron detachment, which indeed become important for ion energies exceeding 10 eV (see Fig. 3). Then, any attempts to calculate the mobility at E/N values higher than about 400 Td should be accompanied by a full consideration of the cross sections for the above inelastic processes. This is well illustrated in Fig. 7(b), showing the SF_6^- energy distribution function for $E/N=2000$ Td, and also in Fig. 8, where the extreme case for $E/N=4000$ Td is shown.

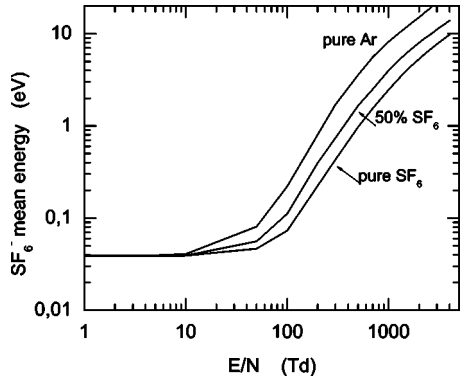

FIG. 8. The mean energy of SF_6^- in SF_6, Ar, and the SF_6-Ar (50:50) mixture as a function of E/N.

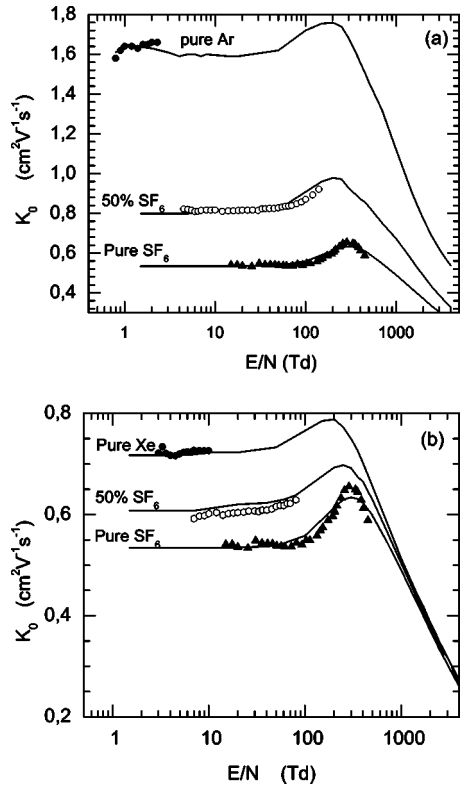

FIG. 9. (a) Calculated mobility of SF_6^- in SF_6, Ar, and the SF_6-Ar (50:50) mixture over a wide E/N range. The symbols are the measured mobilities. The mobilities for pure SF_6 were taken from Ref. [6]. (b) Calculated mobility of SF_6^- in SF_6, Xe, and the SF_6-Xe (50:50) mixture over a wide E/N range. The symbols are the measured mobilities. The mobilities for pure SF_6 were taken from Ref. [6].

Once the selected and calculated collision cross section sets have been validated on the grounds of a very successful agreement between measurement and calculation of the mobility of SF_6^- in the SF_6-Ar and SF_6-Xe mixtures, it is worth pointing out that for the purpose of understanding and modeling of electrical discharges requires the calculation of the mobility and diffusion coefficients over a very wide range of E/N, using the present Monte Carlo code. Thus we have extended the E/N range up to 4000 Td, as is shown in Figs. 9(a) and 9(b) for the calculated mobilities of SF_6^- in SF_6, Ar (or Xe), and SF_6-Ar (or Xe) (50:50). Furthermore, the ratios between the transverse or longitudinal diffusion coefficients and the ion mobility, D_T/K and D_L/K, are plotted in Figs.

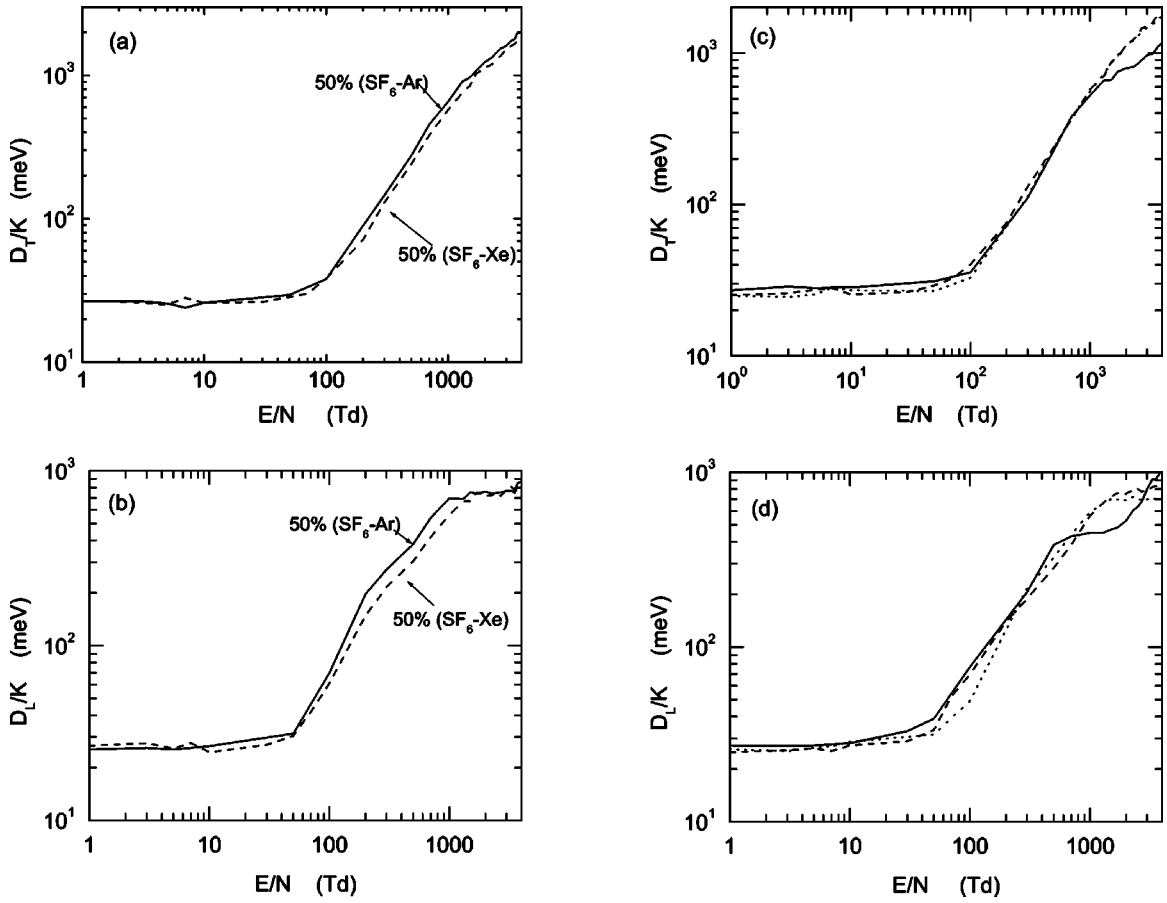

FIG. 10. (a) Calculated D_T/K ratio of SF_6^- in the SF_6-Ar (50:50) and SF_6-Xe (50:50) mixtures as a function of E/N. (b) Calculated D_L/K ratio for SF_6^- in the SF_6-Ar (50:50) and SF_6-Xe (50:50) mixtures as a function of E/N. (c) Calculated D_T/K ratio for SF_6^- in SF_6, Ar, and Xe as a function of E/N. (—) pure Ar; (· · ·) pure SF_6;(---) pure Xe. (d) Calculated ratio D_L/K for $SF_6^-SF_6$, Ar, and Xe as a function of E/N. (—) pure Ar; (· · ·) pure SF_6; (---) pure Xe.

10(a) and 10(b), respectively, for the mixtures SF_6-Ar (50:50) and SF_6-Xe (50:50). Moreover, these values of D_T/K and D_L/K are also shown for pure Ar, Xe, and SF_6 in Figs. 10(c) and 10(d). The behavior of the diffusion coefficient is qualitatively the same in both the pure gas and in the gas mixture, and its dependence with E/N can be explained essentially from the same physical grounds as has been done previously for the ion mobility. Since the diffusion coefficients are inversely proportional to Q_m, this means that the diffusion coefficients of SF_6^- in SF_6-Ar are as expected higher than those for SF_6^- in SF_6-Xe, because the Q_m magnitude of SF_6^--Ar is lower than the Q_m one of SF_6^--Xe, as is seen in Figs. 3(b) and 3(c).

In order to validate, at least partially, the inelastic cross sections used for the present calculations of transport coefficients, the reaction coefficients for formation of SF_5^- from SF_6^-, and of electron detachment from SF_6^- were calculated for the SF_6^--SF_6 system, and are shown in Fig. 11 along with the reaction coefficients measured by different authors [25–27]. It is seen from this figure that both calculated and measured reaction coefficients follow a similar trend, although there exists a fairly large quantitative discrepancy at both ends of the E/N range covered in the calculation for the ion conversion coefficient, which may be attributed to the kinetics model used to deduce the reaction coefficients from drift tube data obtained by O'Neill and Craggs [25]. Indeed, their simplified kinetics model ([25]) did not consider the particular case of ion conversion from SF_6^- to F^- [10], which is quite significant [see Fig. 3(a)]. Nevertheless, it is worth noting that slight changes in the extrapolated cross sections

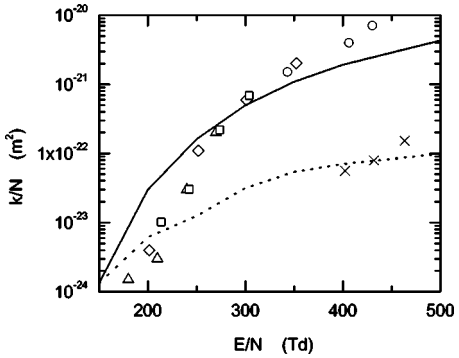

FIG. 11. Reaction coefficients for SF_6^- ion conversion to SF_5^- as a function of E/N. Solid line: calculation; measurements from different sources: ○ [22]; Δ [23]; □ [24]; ◇ [25]. The reaction coefficient for electron detachment. Dotted line: calculation; measurements: × [22].

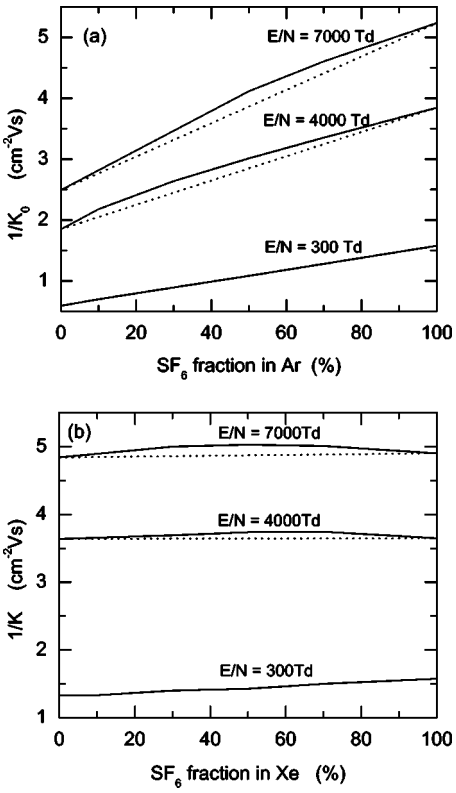

FIG. 12. (a) The inverse of the mobility of SF_6^- in the SF_6-Xe mixtures as a function of the fraction of SF_6 in the mixture. Solid lines : Monte Carlo calculation; dotted lines : calculation from Blanc's law. (b) The inverse of the mobility of SF_6^- in the SF_6-Ar mixtures as a function of the fraction of SF_6 in the mixture. Solid lines : Monte Carlo calculation; dotted lines : calculation from Blanc's law.

at low energies affects significantly the reaction coefficient, but not the mobility of SF_6^-.

B. Assessment of the linear approximation in gas mixtures

In gas mixtures, the ion mobility is usually calculated from macroscopic, classical approximations, as, for example, from Blanc's law

$$\frac{1}{K_{\mathrm{mix}}} = \sum_n \frac{x_n}{K_n}, \tag{16}$$

where x_n is the mole fraction of gas species n in the mixture, and K_n is the corresponding ion mobility in such pure gas. In spite of its fairly widespread use for calculating the ion mobility in a gas mixture, one must be well aware that the above equation is valid only over the low E/N regime. This macroscopic relation has been derived on the assumption that elastic collisions are the only ion-neutral interaction process, where the ion distribution is Maxwellian. Thus these fairly strong approximations restrict the use of Blanc's law to values of E/N where the polarization part of the interaction potential is predominant, and for ion-neutral systems in which the individual energy distribution functions are Maxwellian with the same order of magnitude for all the gaseous components of the mixture. On the other hand, the classical Blanc's law [Eq. (16)] must be corrected after a more or less complex formalism, generally based on the momentum transfer theory in a great deal of cases. Indeed, such corrections are needed either in the presence of only elastic collisions at higher E/N (see, e.g., Refs. [28]), or in the presence of both elastic and inelastic processes at any E/N value (see the recent work of Jovanovic *et al.* [29]). However, the Monte Carlo method remains to be the most direct and rigorous way to obtain the ion transport parameters in gas mixtures provided the ion-gas collision cross sections are available for each individual component of the mixture. Figures 12(a) and 12(b) show the inverse reduced mobility of SF_6^- in SF_6-Ar and SF_6-Xe as a function of the SF_6 fraction, respectively, for several values of E/N. Indeed, these figures show a good linearity at low reduced fields (for example, $E/N = 300$ Td), but an increasing deviation from the Blanc's law as E/N rises.

V. CONCLUSION

The elastic collision cross sections have been calculated for the collision systems SF_6^--SF_6, SF_6^--Ar, and SF_6^--Xe from a semiclassical JWKB approximation based on a rigid core potential model, well adapted for polyatomic interaction systems, while the inelastic cross sections were taken from literature. The cross sections sets used have been validated from the good agreement found between those calculated from a Monte Carlo simulation for SF_6^- ion transport and the measurements based on a time-resolved pulsed Townsend technique.

To the best of our knowledge, the present measurements of the mobility of SF_6^- in the SF_6-Ar and SF_6-Xe mixtures are the first to be reported, and were found in good agreement with those calculated within ±3%, well within our experimental uncertainties. Following this, we have extended our range of calculation of the mobility and the ratios between the diffusion (transverse and longitudinal) and the mobility up to $E/N = 4000$ Td.

Finally, the classical, linear, Blanc's law used in gas mixtures to determine SF_6^- mobility data is compared to present Monte Carlo calculations in both SF_6-Ar and SF_6-Xe mixtures. Significant deviations were found more particularly in the case of SF_6-Ar mixtures for E/N higher than several hundreds of Td when the ion distribution is no longer Maxwellian.

ACKNOWLEDGMENTS

This work was partially supported by DGAPA-UNAM, IN 104501, and UAM-2250216. Thanks are due to A. Bustos for his technical assistance.

[1] T. H Teich, *Electron and Ion Swarms* (Pergamon, New York, 1981), p. 241.
[2] L. G. Christophorou and J. K. Olthoff, J. Phys. Chem. Ref. Data **29**, 267 (2000).
[3] L. G. Christophorou, J. K. Olthoff, and D. S. Green, "Gases for Electrical Insulation and Arc Interruption: Possible Present and Future Alternatives to Pure SF_6," NIST Technical Note 1425, 1997; L. G. Christophorou and R. J. Van Brunt, IEEE Trans. Dielectr. Electr. Insul. **2**, 952 (1999).
[4] N. Nakano, N. Shimura, Z. L. Petrovic, and T. Makabe, Phys. Rev. E **49**, 4455 (1994).
[5] L. G Christophorou, *Electron-Molecule Interactions and their Applications* (Academic, Orlando, FL, 1984), 2 Vols.
[6] A. V. Phelps and R. J. Van Brunt, J. Appl. Phys. **64**, 4269 (1988).
[7] S. R. Hunter, J. G. Carter, and L. G. Christophorou, J. Chem. Phys. **90**, 4879 (1989).
[8] J. de Urquijo, "Ion motion in dielectric gases," *9th International Symposium on Gaseous Dielectrics*, Maryland, EUA, 2001.
[9] J. de Urquijo, I. Alvarez, C. Cisneros, and H. Martínez, in *Nonequilibrium Effects in Ion and Electron Transport*, edited by J. W. Gallagher (Plenum, New York, 1990), pp. 211–227; E. Basurto and J. de Urquijo, Phys. Rev. E **64**, 026412 (2001).
[10] Y. Wang, R. L. Champion, and L. D. J. Doverspike, J. Chem. Phys. **91**, 2254 (1989); J. K. Olthoff, R. J. Van Brunt, Yicheng Wang, R. L. Champion, and D. L. Doverspike, *ibid.* **91**, 2261 (1989).
[11] M. Yousfi, A. Hennad, and O. Eichwald, J. Appl. Phys. **84**, 107 (1998).
[12] H. Raether, *Electron Avalanches and Breakdown in Gases* (Butterworth, London, 1964).
[13] J. de Urquijo, C. Arriaga, I. Alvarez, and C. Cisneros, J. Phys. D **32**, 41 (1999).
[14] J. de Urquijo, I. Alvarez, and C. Cisneros, J. Phys. D **18**, 29 (1985).
[15] G. Hinojosa and J. de Urquijo, J. Phys. D **36**, 2510 (2003); J. de Urquijo and F. B. Yousif, Phys. Rev. E **68**, 046406 (2003).
[16] E. Basurto, G. Hinojosa, J. L. Hernández-Ávila, and J. de Urquijo, *XVI European Conference on Atomic and Molecular Physics of Ionized Gases, Grenoble, France, 2002*, Conference Proceedings Vol. 1 (European Physical Society, Grenoble, 2002), pp. 79-80.
[17] D. Nelson, M. Benhenni, M. Yousfi, and O. Eichwald, J. Phys. D **34**, 32 (2001).
[18] D. Nelson, M. Benhenni, O. Eichwald, and M. Yousfi, J. Phys. D **94**, 96 (2003).
[19] E. A. Mason, H. O'Hara, and F. J. Smith, J. Chem. Phys. **44**, 3513 (1973).
[20] A. Hennad, O. Eichwald, M. Yousfi, and O. Lamrous, J. Phys. III **7**, 1877 (1997).
[21] M. R. C. McDowell and J. P. Coleman, *Introduction to the Theory of Ion-Atom Collisions* (North-Holland, Amsterdam, 1970); R. E. Johnson, in *Introduction to Atomic and Molecular Collisions* (Plenum Press, New York, 1982).
[22] R. J. Munn, E. A. Mason, and F. J. Smith, J. Chem. Phys. **41**, 3978 (1964).
[23] E. A. Mason and E. W. McDaniel, *Transport Properties of Ions in Gases* (Wiley, New York, 1988), p. 245.
[24] J. P. McGeehan, B. C. O'Neill, A. N. Prasad, and J. D. Craggs, J. Phys. D **8**, 153 (1975).
[25] C. O'Neill and J. D. Craggs, J. Phys. B **6**, 2634 (1973).
[26] J. de Urquijo-Carmona, I. Alvarez, and C. Cisneros, J. Phys. D **19**, L207 (1986).
[27] Y. Nakamura and T. Kizu, *Proceedings of 5th International Swarm Seminar, Birmingham, UK* (Springer-Verlag, London, 1987), p.126.
[28] E. A. Mason and H. Hahn, Phys. Rev. A **5**, 438 (1972); H. B. Milloy and R. E. Robson, J. Phys. B **6**, 1139 (1973); L. A. Viehland and E. A. Mason, Ann. Phys. (N.Y.) **91**, 499 (1975); N. Takata J. Phys. D **18**, 1795 (1985).
[29] J. V. Jovanovic, S. B. Vrhovac, and Z. L. Petrovic, Eur. Phys. J. D **28**, 91 (2004).
[30] J. de Urquijo, I. Alvarez, C. Cisneros, and H. Martinez, J. Phys. D **23**, 778 (1990); **24**, 664 (1991).